Cosmic crystallography in a circle

A.F.F. Teixeira [1]

Centro Brasileiro de Pesquisas Físicas
22290-180 Rio de Janeiro-RJ, Brazil

Abstract

In a circle (an S^1) with circumference 1 assume m objects distributed pseudo-randomly. In the univeral covering manifold R^1 assume the objects replicated accordingly, and take an interval $L > 1$. In this interval, make the normalized histogram of the pair separations which are not an integer. The theoretical (expected) such histogram is obtained in this report, as well as its difference to a similar histogram for non-replicated objects. The whole study is of interest for the cosmic crystallography.

---

[1]teixeira@cbpf.br

1   Introduction

Cosmic crystallography (CC) is a method to unveil the topology of the universe, and initially looked for spikes in a pair separation histogram (PSH) [1]. Since spikes are absent in hyperbolic spaces, it appeared that the method was useless in such spaces. However, it was soon shown that not only a Clifford translation (responsible for a spike) press its fingerprint on a PSH, but also the other isometries of the space [2].

When spikes are absent, the PSH of a ball containing repeated images – the $\phi^m(l)$ – is very similar to that of a ball with same radius and same geometry, but without duplication of images – the $\phi^s(l)$. A suggestion was then made, of studying the difference of the *m*ultiply and the *s*imply connected histograms, $\phi^m(l) - \phi^s(l)$ [3].

To improve the method, *exp*ected functions $\phi^s_{exp}(l)$ were derived to replace the histograms $\phi^s(l)$ obtained from computer simulations, for all three geometries with constant curvature [4]. Graphs of $\phi^m(l) - \phi^s_{exp}(l)$ were obtained, clearly evincing the topology of an euclidian, an elliptic, and a hyperbolic three-space [5]. The contribution of each individual isometry g to a PSH was examined, and normalized histograms $\phi^g(l)$ (defined in ref.[2]) were obtained from computer simulations [5]; these simulations also gave histograms of $\phi^u(l) - \phi^s_{exp}(l)$, a previously unsuspected quantity [6].

Recently the exact (noiseless) functions $\phi^g_{exp}(l)$ were given for the euclidian isometries [7]. In the present report we finally have a first acquaintance with functions $\phi^u_{exp}(l)$, the exact (noiseless) counterparts of the 'uncorrelated' normalized histograms $\phi^u(l)$ defined in [6]. We examine a one-dimensional system: a universe with topology S^1, a circle with circumference 1; we assume the horizon at a distance $L/2$ on each side of an observer, so the visible universe has total length L; clearly if $L > 1$ then there are repeated images in this visible universe. In section 2 we give a detailed description of how to obtain the expected uncorrelated signature $\varphi^u_{L\,exp}(l)$ when $1 < L < 2$. In section 3 we exhibit the generalization for arbitrary horizon $L/2$. In the Conclusion we make a few comments, and in four Appendices we derive a few somehow lengthy mathematical results stated in the report.

2   When $1 < L < 2$

In a computer simulation, we usually execute the following set of prescriptions to obtain the uncorrelated signature $\varphi_L^u(l)$:
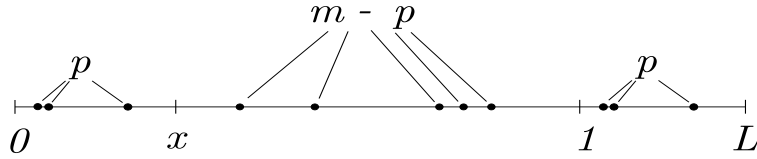

Figure 1 The distribution of objects in the interval $(1, L)$ is an exact copy of the distribution in $(0, x)$; here $p = 3$ and $m = 8$.

1. in an interval $(0, 1)$ randomly distribute m objects; see figure 1;

2. in the side interval $(1, L)$ make an exact replica of the p objects laying in $(0, x)$;

3. measure the $(m + p)(m + p - 1)/2$ separations l between the total $m + p$ objects, and discard the p correlated separations (those which have $l = 1$ exactly);

4. make a normalized histogram of the

$$\mathcal{D}_{mp} = \frac{1}{2}(m + p)(m + p - 1) - p \qquad (1 < L < 2) \tag{1}$$

   uncorrelated separations;

5. make a large number of new normalized histograms, by repeating the steps 1 to 4 with same m (although p usually varies);

6. take the mean of these histograms, $< \phi_{mL}^u(l) >$, and construct the quantity

$$< \varphi_{mL}^u(l) > = (n - 1 - \sum_{g \in \tilde{\Gamma}} \nu_g)\Big[< \phi_{mL}^u(l) > - \phi_L^s(l)\Big], \tag{2}$$

   where

$$\phi_L^s(l) = \frac{2}{L}(1 - \frac{l}{L}), \quad 0 < l < L, \tag{3}$$

   and where the factor $n - 1 - \sum \nu_g = (m - 1)L - x(1 - x)/L$ is explained in the appendix 1;

7. the (computer simulated) *uncorrelated* signature $< \varphi_L^u(l) >$ is the quantity $< \varphi_{mL}^u(l) >$ when $m \to \infty$; in practice $m > 50$ usually suffices. See figure 2.

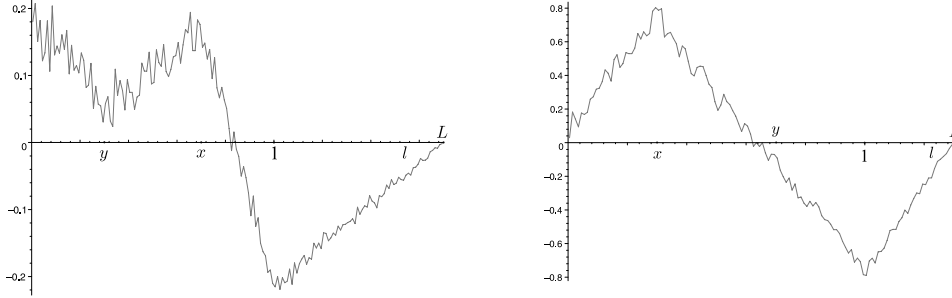**Figure 2** Computer simulated functions $< \varphi_{mL}^u(l) >$ for $\{m = 2, L = 1.7\}$ and $\{m = 30, L = 1.3\}$.

We now develop an analytical method to obtain the uncorrelated signature $\varphi_L^u(l)$. We are dropping the subscript *exp* in all expected (theoretic, analytic, mean) probability distributions. Initially define the lengths x and y (see figure 1)

$$x = L - 1, \quad y = 1 - x \quad (1 < L < 2), \tag{4}$$

and assume that m objects are randomly distributed in $(0, 1)$; the probability that p objects be in the interval $(0, x)$ and $m - p$ objects be in the interval $(x, 1)$ clearly is

$$\mathcal{P}_{mpx} = C_m^p x^p y^{m-p}, \quad C_m^p = \frac{m!}{p!(m-p)!}; \tag{5}$$

irrespective of the values of m and x we have

$$\sum_{p=0}^m \mathcal{P}_{mpx} = 1. \tag{6}$$

We denote as $\phi_{mpL}^u(l)dl$ the probability of finding in $(0, L)$ an uncorrelated pair with separation between l and $l + dl$, when there are m objects in $(0, 1)$ and p objects in $(0, x)$; clearly it satisfies

$$\int_0^L \phi_{mpL}^u(l)dl = 1. \tag{7}$$

Recall that a pair (P, Q) is said g-correlated when the isometry g brings one of the members to the other; the pair is uncorrelated when no such g exists. To investigate $\phi_{mpL}^u(l)$ when $1 < L < 2$ we first call A the interval $(0, x)$, call $B = (x, 1)$, and call $C = (1, L)$, and note that there are

- $w_{AA} = p(p-1)/2$ pairs with both members in A;

- $w_{AB} = p(m-p)$ pairs with a member in A and the other in B;

- $w_{AC} = p(p-1)$ uncorrelated pairs, with a member in A and the other in C;

- $w_{BB} = (m-p)(m-p-1)/2$ pairs with both members in B;

- $w_{BC}(= w_{AB})$ pairs with a member in B and the other in C;

- $w_{CC}(= w_{AA})$ pairs with both members in C.

In total , there are $\mathcal{D}_{mp}$ (eq.(1)) pair separations to be considered.

A short reflection gives that the density $\phi^u_{mpL}(l)$ can be decomposed as

$$\phi^u_{mpL}(l) = \frac{1}{\mathcal{D}_{mp}} \Big[w_{AA}\phi_{AA}(l) \;\; + \;\; w_{AB}\phi_{AB}(l) + w_{AC}\phi_{AC}(l) + $$
$$w_{BB}\phi_{BB}(l) \;\; + \;\; w_{BC}\phi_{BC}(l) + w_{CC}\phi_{CC}(l) \Big], \tag{8}$$

where each $\phi_{XY}(l)$ is the probability density of finding an uncorrelated pair of objects separated by l, one in X and the other in Y; clearly all obey

$$\int_0^L \phi_{XY}(l)dl = 1. \tag{9}$$

There are two basic types of $\phi_{XY}(l)$, according as $X = Y$ or $X \neq Y$. When $X = Y$, suppose a segment of length μ, and randomly select two points of it; the probability that their separation lie between l and $l + dl$ is $\phi^s_\mu(l)dl$ with (see figure 3)

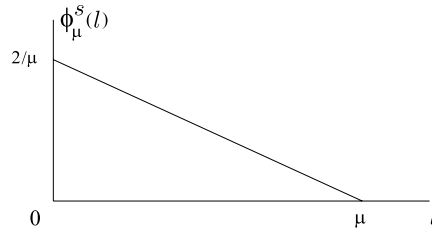$$\phi^s_\mu(l) = \frac{2}{\mu}(1 - \frac{l}{\mu}), \quad 0 < l < \mu. \tag{10}$$

Figure 3 Pair separation density function for an interval μ. The underlying area is 1.

When $X \neq Y$, consider two intervals with lengths α and β, with separation δ (see figure 4); randomly select one point in each α and β; the probability that the separation between these points lie between l and $l + dl$ is $\phi_{\delta(\alpha\beta)}(l)dl$, with the density $\phi_{\delta(\alpha\beta)}(l)$ as depicted in figure 5.
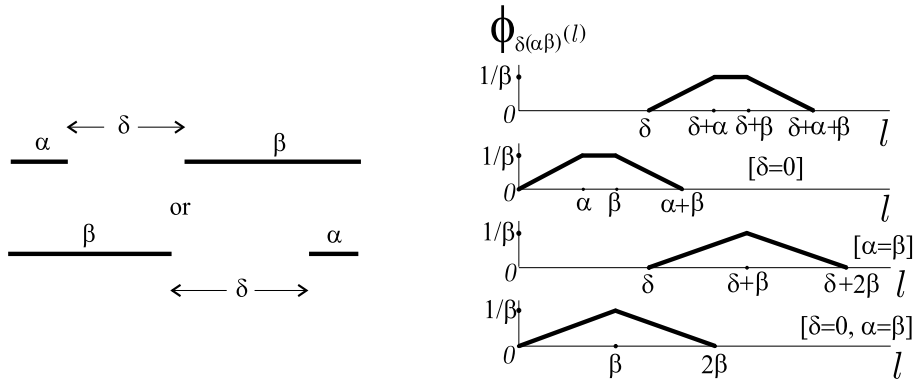
.

Figure 4 Intervals with lengths α and β, with separation δ; assume $\alpha \leq \beta$.

Figure 5 The probability density $\phi_{\delta(\alpha\beta)}(l)$ for $\alpha \leq \beta$ (see figure 4); three particular cases are also displayed; all underlying areas are $= 1$.

The functions $\phi_{XY}(l)$ appearing in eq.(8) are as displayed in the figure 6, for the case with $x \leq y$; for $x \geq y$ a similar set has to be constructed, see figure 7.
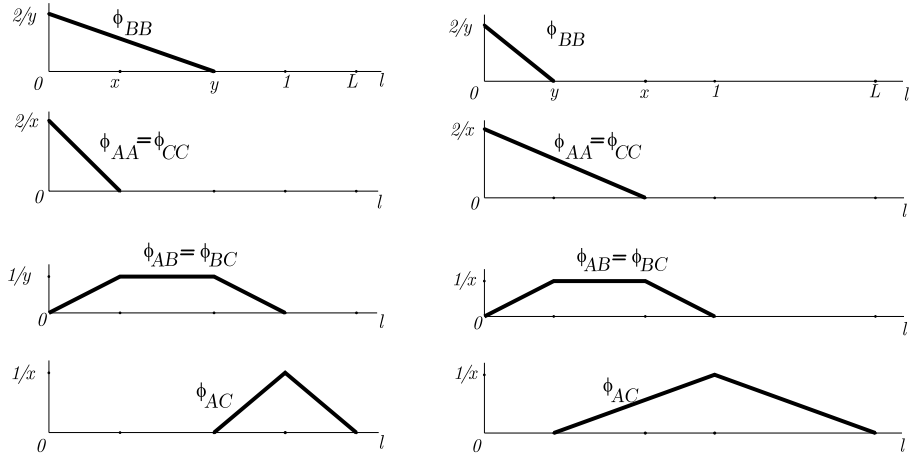
Figure 6 The normalized functions $\phi_{XY}(l)$ when $1 < L < 2$ and $x \leq 0.5$.

Figure 7 The same functions when $x \geq 0.5$.

When $x \leq 0.5$ the density $\phi^u_{mpL}(l)$, eq.(8), is a sequence of four straight segments with endpoints at $l = 0, x, y, 1$, and L (in this order), and values

$$
\begin{aligned}
\phi^u_{mpL}(0) &= \frac{1}{\mathcal{D}_{mp}}[w_{BB}\frac{2}{y} + 2w_{AA}\frac{2}{x}], & (11)\\
\phi^u_{mpL}(x) &= \frac{1}{\mathcal{D}_{mp}}[w_{BB}\frac{2(y-x)}{y^2} + 2w_{AB}\frac{1}{x}] \quad (x \leq 0.5),\\
\phi^u_{mpL}(y) &= \frac{1}{\mathcal{D}_{mp}}[2w_{AB}\frac{1}{y}] \quad (x \leq 0.5),\\
\phi^u_{mpL}(1) &= \frac{1}{\mathcal{D}_{mp}}[w_{AC}\frac{1}{x}], \quad \phi^u_{mpL}(L) = 0.
\end{aligned}
$$

When $x \geq 0.5$ the sequence of endpoints changes to $l = 0, y, x, 1$, and L, and the values of $\phi^u_{mpL}(l)$ at $l = y$ and $l = x$ become

$$
\begin{aligned}
\phi^u_{mpL}(y) &= \frac{1}{\mathcal{D}_{mp}}[2w_{AA}\frac{2(x-y)}{x^2} + 2w_{AB}\frac{1}{x}] \quad (x \geq 0.5) & (12)\\
\phi^u_{mpL}(x) &= \frac{1}{\mathcal{D}_{mp}}[2w_{AB}\frac{1}{x} + w_{AC}\frac{x-y}{x^2}] \quad (x \geq 0.5).
\end{aligned}
$$

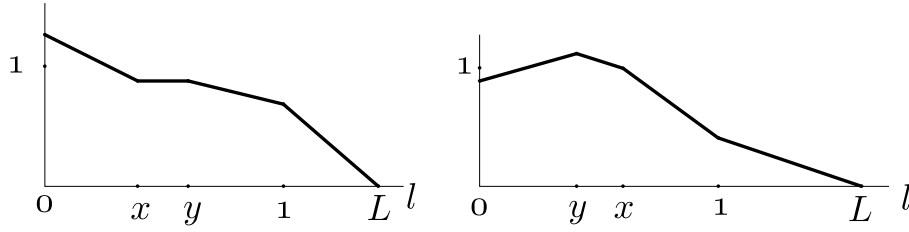Two examples of functions $\phi^u_{mpL}(l)$ for $1 < L < 2$ are shown in figure 8.

Figure 8 The probability density $\phi^u_{mpL}(l)$ for $m = 3, p = 2$, and two values of L: 1.4 and 1.6 . Both underlying areas are 1.

Having the $m + 1$ functions $\phi^u_{mpL}(l)$, $p = 0, ..., m$, we introduce the probability density

$$\phi^u_{mL}(l) = \sum_{p=0}^{m} \mathcal{P}_{mpx} \phi^u_{mpL}(l), \tag{13}$$

whose interpretation is obvious: $\phi^u_{mL}(l)dl$ is the probability that two uncorrelated objects randomly selected in L have separation between l and $l+dl$, when m objects were randomly distributed in the interval (0, 1). Examples of $\phi^u_{mL}(l)$ are given in figure 9.
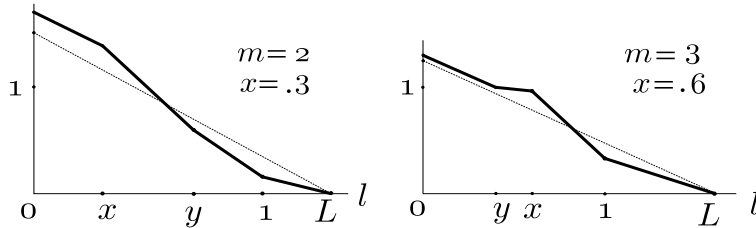

Figure 9 Probability densities $\phi^u_{mL}(l)$ for $1 < L < 2$. The graph of $\phi^s_L(l)$ is given in dotted line, for comparison.

Cosmic crystallography is mostly interested in systems with $m >> 1$. In this limit the function $\phi^u_{mL}(l)$ closely resembles the simple triangular function $\phi^s_L(l)$ (eq.(3), fig. 3), so one is led to define the difference

$$\varphi^u_L(l) = \lim_{m \to \infty} mL\Big[\phi^u_{mL}(l) - \phi^s_L(l)\Big], \tag{14}$$

the asymptotic uncorrelated signature of L.

We soon find that the function $\varphi_L^u(l)$ has a number of symmetries:

$$\varphi_L^u(0) = \varphi_L^u(L/2) = \varphi_L^u(L) = 0, \quad \varphi_L^u(x) = -\varphi_L^u(1). \tag{15}$$

In other words, every $\varphi_L^u(l)$ with $1 < L < 2$ is composed of three line segments, with the first segment parallel to the third (see figure 10). As expected, the entire graph of $\varphi_L^u(l)$ is uniquely fixed by the number $f(L)$, the value of $\varphi_L^u(l)$ at $l = x$; in the appendix 2 we show that

$$f(L) = \frac{8xy}{L^3} \quad (1 < L < 2). \tag{16}$$

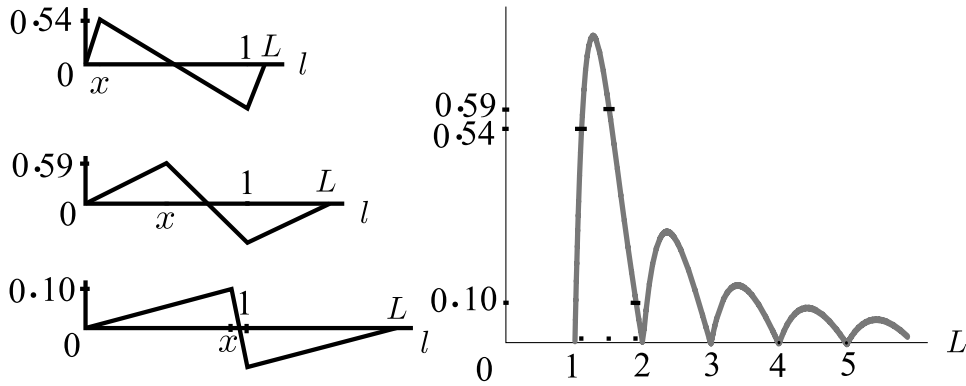A plot of $f(L)$ valid for arbitrary $L > 1$ is given in figure 11.

Figure 10 Geometro-topological signature $\varphi_L^u(l)$ for $L =1.1$, 1.5, and 1.9 .

Figure 11 The function $f(L)$, the absolute maximum of $\varphi_L^u(l)$ (which occurs at $l = x$); three particular values of L are marked, those used in figure 10.

3   When $L > 2$

The generalization of the previous results for arbitrary values of L is straightforward but lengthy, so we only state the final results in this section. See the appendix 3 for details. The graph of the uncorrelated signature (14) with

$$L = \lambda + x, \quad \lambda \in Z_+, \quad 0 < x < 1 \tag{17}$$

has the aspect of a slanted saw; see figure 12, drawn for $\lambda = 5$ and $x = 0.2$.
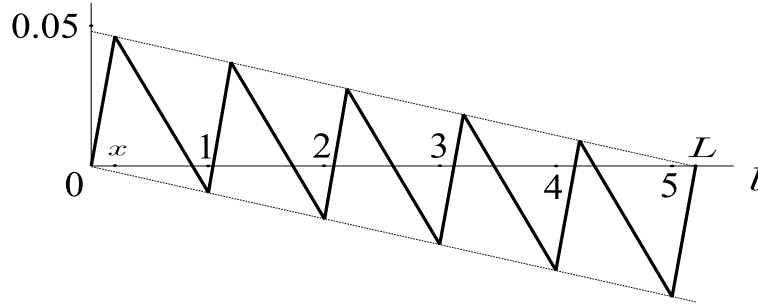
.

Figure 12 The function $\varphi_L^u(l)$ for $L = 5.2$.

There are λ maxima, which occur in the positions $l = x, 1 + x, ..., (\lambda - 1) + x$, and there are λ minima, which lay in the positions $l = 1, 2, ..., \lambda$. A straight line connects the maxima, another one connects the minima, both have angular coefficient $-8xy/L^3$. The $\lambda + 1$ segments with positive angular coefficient are parallel, as well as the λ segments with negative slope. As expected, the value of L is the sufficient datum to draw $\varphi_L^u(l)$, since

$$\varphi_L^u(x) = -\varphi_L^u(\lambda) = \frac{8\lambda xy}{L^3},\tag{18}$$

as shown in the appendix 4. The graph of $f(L) = 8\lambda xy/L^3$ is given in Figure 11.

4 Conclusion

In our first contact with the cosmic crystallography it appeared plausible that the normalized expected functions $\phi_{exp}^u(l)$ and $\phi_{exp}^s(l)$ were the same, since both are concerned with separations between objects isometrically unrelated [2]. However, in our computer simulations a persistent non-nullity of the difference $< \phi^u(l) > -\phi_{exp}^s(l)$ made imperative a more close exam. It soon became evident that a difference indeed existed, and that it diminished as the number n of objects present in the sample increased.

Further investigation suggested to define the uncorrelated signature [6]

$$\varphi_{exp}^u(l) = (n - 1 - \sum \nu_g)\Big[\phi_{exp}^u(l) - \phi_{exp}^s(l)\Big],\tag{19}$$

where $\nu_g = N_g/n$, with N_g =number of g-pairs in the observed universe; for the cosmic crystallography we usually have $n >> 1 + \sum \nu_g$.

Earlier attempts to find $\phi^u_{exp}(l)$ for three-dimensional balls failed, and also for $2D$ balls; we then focussed our attention on a $1D$ ball, this report. When we compare the final theoretical result (14) with the mean of an increasing number of histograms obtained from computer simulations, we note a rapid agreement of the two approaches in the region of large separations $l > L/2$, while in the region where $l < L/2$ a quite larger number of simulated catalogs is demanded. This can be seen in Figure 2, where we observe that the statistical fluctuations for l large are sensibly less pronounced than those for small l.

When $L < 1$, then there is no replication of objects; in this case $\phi^u_L(l) = \phi^s_L(l)$ and clearly $\varphi^u_L(l) = 0$. When $L > 1$ is an integer, then objects are replicated; nevertheless still $\phi^u_L(l) = \phi^s_L(l)$ and $\varphi^u_L(l) = 0$. This can be seen in the figure 11, where we note that $f(L)$ vanishes for $L =$ integer > 0.

Appendix 1

We evaluate the quantity $n - 1 - \sum \nu_g$ for a universe S^1 with circumference 1 and observed universe with total amplitude $L = \lambda + x$, being λ a positive integer and $0 < x < 1$.

Assuming m objects along the circle S^1 with radius $1/(2\pi)$, then the expected number of objects in L is $n = mL$. The sum $\sum \nu_g = \nu_{-\lambda} + \nu_{-\lambda+1} + ... + \nu_{-1} + \nu_1 + ... + \nu_{\lambda-1} + \nu_\lambda$ indeed simplifies to $2(\nu_1 + \nu_2 + ... + \nu_\lambda)$, since $\nu_{-i} = \nu_i$.

Now remember that for i a positive integer $n\nu_i$ is the expected number of pairs of objects in the observed universe whose separation is $i \leq \lambda$ [2]; its value is

$$n\nu_i = m(L - i). \tag{20}$$

As a consequence $\sum \nu_g = \lambda(L - y)/L$, and finally

$$n - 1 - \sum \nu_g = (m - 1)L - \frac{xy}{L}. \tag{21}$$

Appendix 2

We show that $\varphi_L^u(x) = 8xy/L^3$ when $1 < L < 2$: from (11) or (12) we have at $l = 1$

$$\phi_{mpL}^u(1) = \frac{1}{\mathcal{D}_{mp}} \frac{p(p-1)}{x}, \tag{22}$$

so we have from (13)

$$\phi_{mL}^u(1) = \frac{1}{x} \sum_{p=0}^{m} \frac{\mathcal{P}_{mpx}}{\mathcal{D}_{mp}} p(p-1), \tag{23}$$

whose value is sought, correct to order m^{-1} when $m >> 1$. In this limit we have

$$\sum_{p=0}^{m} \mathcal{P}_{mpx}(p/m)^k = x^k + \frac{k(k-1)}{2m} y\, x^{k-1} + O(m^{-2}), \tag{24}$$

and consequently

$$\sum_{p=0}^{m} \mathcal{P}_{mpx} F(p/m) = F(x) + \frac{xy}{2m} \frac{d^2}{dx^2} F(x) + O(m^{-2}). \tag{25}$$

For $m >> 1$ in eq.(1) we find that

$$\frac{p(p-1)}{\mathcal{D}_{mp}} = \frac{2\xi^2}{(\xi+1)^2} + \frac{2\xi(2\xi+1)(\xi-1)}{m(\xi+1)^4} + O(m^{-2}), \quad \xi := p/m, \tag{26}$$

so from (25) we obtain

$$\sum_{p=0}^{m} \mathcal{P}_{mpx} \frac{p(p-1)}{\mathcal{D}_{mp}} = \frac{2x^2}{(1+x)^2} + \frac{2x(2x+1)(x-1)}{m(1+x)^4} + \frac{xy}{2m} \frac{d^2}{dx^2} \Big[\frac{2x^2}{(1+x)^2} \Big] + O(m^{-2})$$

$$= \frac{2x^2}{L^2} - \frac{8x^2 y}{mL^4} + O(m^{-2}). \tag{27}$$

Since $\phi_L^s(1) = 2x/L^2$, we finally have from (14), (23), and (27)

$$\varphi_L^u(1) = -\frac{8xy}{L^3} \quad (1 < L < 2). \tag{28}$$

Appendix 3

We generalize for arbitrary $L > 1$ the results obtained for $1 < L < 2$, in particular the equations (1) and (16). We first decompose the total interval $(0, L)$ into $2\lambda+1$ subintervals according to figure 13, drawn for $\lambda = 5$.
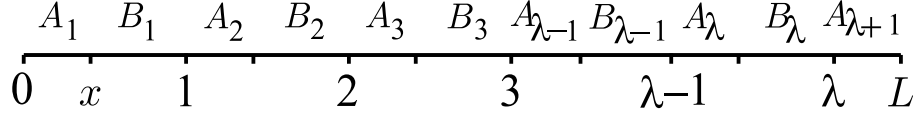

Figure 13 The one-dimensional observed universe with length $L = \lambda + x$, partitioned into $\lambda+1$ intervals A_i with length x and λ intervals B_i measuring $y = 1 - x$.

For m objects randomly distributed in the universe $(0, 1)$ we expect $p = mx$ objects in each interval A_i and $m - p = my$ objects in each B_i. The number of objects in the observed universe $(0, L)$ being $m\lambda + p$, the total number of pairs of objects in it is $(m\lambda + p)(m\lambda + p - 1)/2$; if we deduct the $p\lambda(\lambda + 1)/2$ correlated pairs with members in the A's, and the $(m - p)(\lambda - 1)\lambda/2$ correlated pairs with members in the B's, then we obtain the expected number of uncorrelated separations (cf eq.(1)):

$$\mathcal{D}_{mp} = \frac{1}{2}(m\lambda + p)(m\lambda + p - 1) - \frac{1}{2}\lambda(\lambda + 1)p - \frac{1}{2}\lambda(\lambda - 1)(m - p). \qquad (29)$$

We next note in $(0, L)$ the existence of

- $w_{A_i A_i} = p(p - 1)/2$ pairs with both members in A_i;

- $w_{B_i B_i} = (m - p)(m - p - 1)/2$ pairs with both members in B_i;

- $w_{A_i A_{j>i}} = 2w_{A_i A_i}$ uncorrelated pairs, with a member in A_i and the other in $A_{j>i}$;

- $w_{B_i B_{j>i}} = 2w_{B_i B_i}$ uncorrelated pairs, with a member in B_i and the other in $B_{j>i}$;

- $w_{A_i B_{j\geq i}} = p(m - p)$ pairs, with a member in A_i and the other in $B_{j\geq i}$;

- $w_{B_i A_{j>i}} = w_{A_i B_{j\geq i}}$ pairs, with a member in B_i and the other in $A_{j>i}$.

There is a total of $(2\lambda + 1)(\lambda + 1)$ such numbers w_{XY}, and their sum clearly is the $\mathcal{D}_{mp}$ given in (29).

With the probability densities $\phi_{XY}(l)$ defined as before, the normalized probability density $\phi_{mpL}^u(l)$ is written similarly to eq. (8),

$$\phi_{mpL}^u(l) = \frac{1}{\mathcal{D}_{mp}} \sum_{X,Y} w_{XY} \phi_{XY}(l). \tag{30}$$

As a matter of fact, there are only three essentially different w_{XY}, which we dub w_{AA}, w_{AB}, and w_{BB}, as in sec. 2. Also, there are indeed only $3\lambda + 1$ different functions $\phi_{XY}^{\neq}(l)$, each appearing with variable multiplicity m_{XY}. These functions, together with the corresponding m_{XY} and weights w_{XY}, are displayed in figure 14, drawn for $L = 5.2$.
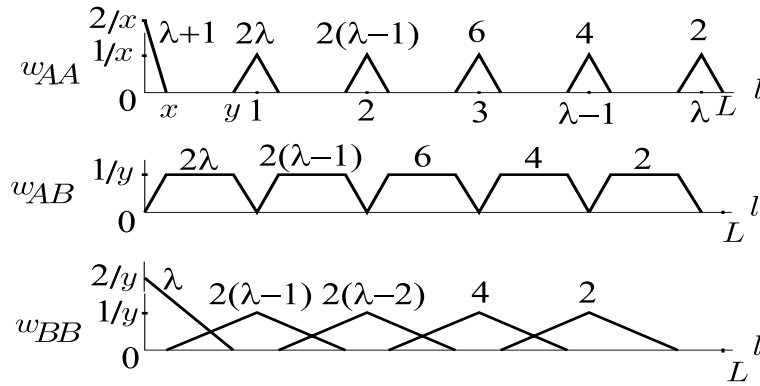

Figure 14 The $3\lambda + 1$ different functions $\phi_{XY}^{\neq}(l)$ when $x \leq 0.5$. On top of each function the corresponding multiplicity m_{XY} is written. On the left side the corresponding weight w_{XY} is also given. The value $L = 5.2$ was taken for definiteness.

When $x > 0.5$ the set of functions $\phi_{XY}^{\neq}(l)$ has a different aspect; see figure 15, drawn for $L = 5.8$.
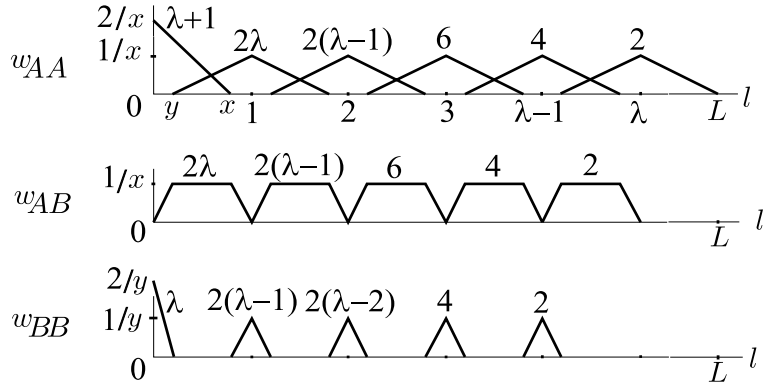
Figure 15 The $3\lambda + 1$ different functions $\phi_{XY}^{\neq}(l)$ when $x \geq 0.5$. The multiplicities m_{XY} and weights w_{XY} are indicated as in figure 14. The value $L = 5.8$ was taken for definiteness.

It is now clear that the functions $\phi_{mpL}^{u}(l)$ are a sequence of $3\lambda + 1$ segments, each segment having endpoints either at an integer or separated x from an integer; as a consequence, also the functions $\phi_{mL}^{u}(l)$ (eq.(13)) have that behavior, as well as the functions $\varphi_{mL}^{u}(l)$ (eq.(2)). See figure 16.
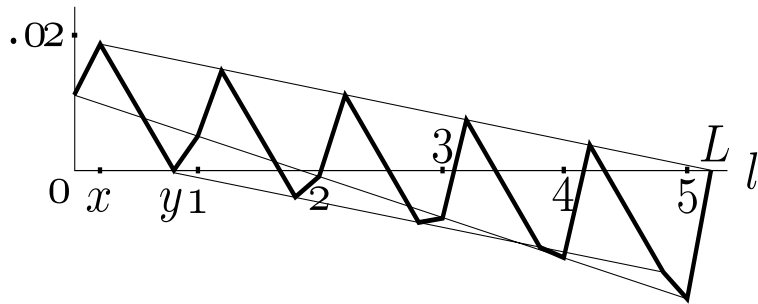

Figure 16 The function $\varphi_{mL}^{u}(l)$ for $m = 2$ and $L = 5.2$. A straight line connects the points with abscissa $l = i + x \, (i = 0, ..., \lambda)$; another, parallel, connects those with $l = i + y \, (i = 0, ..., \lambda - 1)$; also the points with $l =$ integer are aligned.

Appendix 4

We generalize eq.(28) for arbitrary $L > 1$. For $m >> 1$ and $\mathcal{D}_{mp}$ as in eq.(29) we have

$$\frac{p(p-1)}{\mathcal{D}_{mp}} = \frac{2\xi^2}{(\xi + \lambda)^2} + \frac{2\lambda\xi(2\xi + \lambda)(\xi - 1)}{m(\xi + \lambda)^4} + O(m^{-2}), \tag{31}$$

while eq.(27) now reads

$$\phi_{mL}^u(\lambda) = \frac{2x^2}{L^2} - \frac{8\lambda x^2 y}{mL^4} + O(m^{-2}).$$

(32)

Finally (28) becomes

$$\varphi_L^u(\lambda) = -\frac{8\lambda xy}{L^3}, \quad L > 1.$$

(33)

The graph of $f(L) = 8\lambda xy/L^3$ is given in figure 11.

Acknowledgments

References

[1] R. Lehoucq, M. Lachièze-Rey, and J.-P. Luminet, *Cosmic crystallography*, Astron. Astroph. **313**, 339-346 (1996).

[2] G.I. Gomero, A.F.F. Teixeira, M.J. Rebouças and A. Bernui, *Spikes in cosmic crystallography*, http:// xxx.lanl.gov/ abs/ gr-qc/9811038.

[3] H.V. Fagundes and E. Gausmann, *Cosmic crystallography in compact hyperbolic spaces*, http:// xxx.lanl.gov/ abs/ astro-ph/9811368.

[4] A. Bernui and A.F.F. Teixeira, *Cosmic crystallography: three multipurpose functions*, http:// xxx.lanl.gov/ abs/ astro-ph/9904180.

[5] G.I. Gomero, M.J. Rebouças and A.F.F. Teixeira, *A topological signature in cosmic topology*, http:// xxx.lanl.gov/ abs/ gr-qc/9911049.

[6] Third version of reference [2].

[7] A. Bernui and A.F.F. Teixeira, *Cosmic crystallography: the euclidean isometries*, http:// xxx.lanl.gov/ abs/ gr-qc/0003063.